International Journal of Computational Methods and Experimental Measurements
https://www.acadlore.com/journals/IJCMEM

Numerical Modeling of Supersonic Flow Through a Ramjet Nozzle Using Ansys Fluent

Mustafa Abdulsalam Mustafa, Atheer Raheem Abdullah*, Mohammed Mousa Al-Azzawi

Department of Mechanical Power Techniques Engineering Refrigeration and Air-Conditioning Branch, Al-Rafidain University, 10064 Baghdad, Iraq

* Correspondence: Atheer Raheem Abdullah (atheer_raheem@ruc.edu.iq)

Received: 10-30-2025 **Revised:** 12-12-2025 **Accepted:** 12-24-2025

Citation: M. A. Mustafa, A. R. Abdullah, and M. M. Al-Azzawi, "Numerical modeling of supersonic flow through a ramjet nozzle using Ansys Fluent," *Int. J. Comput. Methods Exp. Meas.*, vol. 13, no. 4, pp. 993–1005, 2025. https://doi.org/10.56578/ijcmem130416.

Abstract: A ramjet nozzle was designed for supersonic operating conditions and evaluated numerically using Ansys Fluent 16.1 over a range of chamber-to-ambient pressure ratios. The nozzle geometry was generated to achieve smooth, shock-free expansion under supersonic outflow conditions using the characteristic curve method at a specific nozzle chamber pressure and temperature using Matrix Laboratory (MATLAB) and then validated by comparing the numerical predictions with available experimental data. The results show that a pressure ratio of 57 provides the highest thrust coefficient (TC), while lower ratios lead to over-expanded flow and higher ratios to under-expansion with increased shock losses. Contours of pressure, temperature, and Mach number confirm the expected supersonic flow structure and demonstrate that the nozzle achieves optimum performance under the identified conditions.

Keywords: Ramjet; Compressible flow; Computational fluid dynamics; Nozzle; Supersonic nozzle

1 Introduction

Ramjet engines are used in high-speed aircraft engines. Historically, these engines are intermediate in the evolutionary chain of conventional jet engines and supersonic scramjet engines [1]. Their design is characterized by the simplicity of their design, as they work through a specific shape to convert the pressure and heat energy generated by combustion into kinetic energy, which is converted into thrust for the aircraft [2].

The nozzle plays a central role in ramjet engine behaves. It helps turn the heat from combustion into pressure and then into the speed needed to create thrust. The flow inside this part is not simple. It moves at supersonic speeds and carries strong changes in temperature and pressure [3]. The conditions of Ramjet engines work are hot, pressurized air, so the nozzle shapes both the thrust and the thermal load. Over the years, different studies looked at how the nozzle performs. Some focused on the flow shapes inside it, and others explored shocks, energy losses, or the heating that reaches the walls. Heiser et al. [1], Neill and Pesyridis [2], and Haidn [4] described the basic role of nozzles in high-speed propulsion. Svoboda [5] discussed high altitudes and limits that we try to work around. Several studies have examined supersonic flow inside nozzles, showing that it is essential to track shock-wave behavior, shock–boundary-layer interaction, and plume development [3, 6, 7]. Thermal and structural aspects of nozzles have explored in a way similiar to realistic conditions. Thongsri et al. [8] and Sheikh et al. [9] examined heat moves through the walls, ablation starts, and thermal stresses. Their results suggest that the highest loads often appear near the throat. The load depend on how the insulation responds and the wall material changes with temperature. Li et al. [10] and Braun and Paniagua [11] also pointed out that cooling methods and integrated geometries offer suffice results when trying to manage temperature in detonation-based propulsion. The shape of the nozzle has its own influence. Zakharov et al. [12] studied the effect of the divergent section changes on the internal shock structure and pressure layout. Other studies turned to combustion stability and the link between the inlet and the nozzle [13–15].These works showed that the flow inside can be quite sensitive to backpressure. Baidya et al. [16] and Naidu and Bajaj [17] added that altitude, external expansion, and reflected shocks can change thrust and wall heating in different ways. In parallel, numerical efforts by Le Pichon and Laverdant [18], Kozelkov et al. [19], Wang et al. [20], and Shieh et al. [21] offered acceptable insights into shock wave, ramp type nozzles, and

expansion-deflection layouts. Wang et al. [22] also showed materials wear by fluid–structure interaction. Across these studies, the focus evaluating of current nozzle shapes or modified designs for different operating conditions.

Some researchers touched on effect of geometry changes but a smaller group worked on creating a full nozzle contour from the ground up. Their aim was to reach a smoother and shock-free supersonic expansion. Building on this body of research, the present study develops such a nozzle contour and evaluates its performance over a range of chamber-to-ambient pressure ratios, aiming to identify the conditions associated with optimal thrust and minimal shock losses.

We note that all previous studies focused on studying pre-designed nozzles for specific engines with specific dimensions and studying the design parameters of the thermal and aerodynamic performance of these nozzles, without providing scientific details on their design. In this research, we will design the required nozzle for a ramjet engine under specific operating conditions using the characteristic curves method to design the divergent portion of the nozzle, ensuring isentropic flow throughout the entire divergent portion of the nozzle. We will also study the effect of changing the compression ratio (chamber to exit pressure ratio) on the thermal performance of this nozzle and the extent to which the aforementioned design is compatible with the characteristic curves' method.

This research aims to design a supersonic ramjet nozzle using a characteristic curve approach to ensure shock-free isentropic expansion at the design pressure ratio, and to study its thermal and pneumatic performance across a wide range of chamber-interface pressure ratios. It also aims to determine the optimal operating conditions for maximum thrust and to analyze the flow behavior under suboptimal operating conditions. The characteristic curves method was analyzed using Matrix Laboratory (MATLAB), while the thermal performance of the proposed design was studied numerically using Ansys Fluent 16.1.

2 Materials and Methods

A ramjet engine is a supersonic engine that operates by converting the pressure energy generated by fuel combustion into the kinetic energy of the combustion gases, which provides the thrust necessary to propel the engine forward. Air enters the engine through an inlet shaped in a way that helps slow it down and raise its pressure. Inside this section, the flow becomes subsonic. After that, it mixes with fuel in the combustion chamber, forming gases at higher pressure and temperature [23].

These gases move toward the exit, which is a convergent–divergent nozzle. This nozzle guides the flow so it leaves at supersonic speed and provides the thrust the engine relies on.

Compared with a conventional jet engine, a ramjet has a simpler layout. It does not include rotating parts which makes it more practical at supersonic speeds. The engine has four main elements: the air inlet, the combustion chamber, the nozzle, and the injection system. The last part helps spread the fuel inside the chamber and offer acceptable combustion results, as shown in Figure 1 [24].

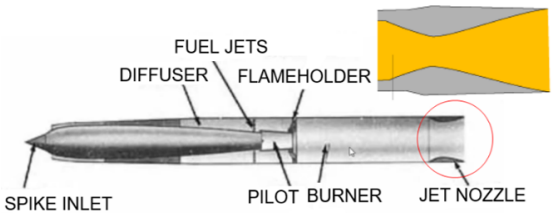

Figure 1. Ramjet operation principles

The main distinction between ramjets and scramjets comes from the air fast inside the combustion chamber and engine work. In a ramjet, the air slows down to subsonic speed before combustion. The engine works reasonably well in the range between about Mach 1 and Mach 5. In a scramjet, the air keeps its supersonic speed through the combustor therefore it run at much higher speeds (Mach 15 or more). In simple terms, ramjets fit the supersonic range, while scramjets are meant for higher speeds, with changes in the combustor and nozzle that help keep the flame stable [25].

The ramjet nozzle is shaped to make good use of the combustion gases and produce the necessary thrust. Its geometry depends on the pressure and temperature inside the chamber. A convergent–divergent layout is used so the gases accelerate to supersonic speed while keeping energy losses at a acceptable level [26]. The design also tries to reduce reflections and flow disturbances inside the nozzle. Materials are chosen to tolerate the high temperatures created during combustio [27].

The design of convergent-divergent nozzles used in rocket engines depends primarily on the chamber pressure-to-back pressure ratio at a specific exit-to-throat nozzle cross-section ratio. When subsonic flow enters the convergent portion of the nozzle, the flow velocity increases and its pressure decreases as shown in the Figure 2. At a specific pressure ratio, the pressure at the nozzle throat decreases to the point where the flow becomes sonic. Below this

pressure ratio, the flow throughout the nozzle remains subsonic. When the pressure at the throat reaches a value that makes the flow at the throat sonic, there are two possibilities: either the flow remains subsonic in the divergent portion, or it transforms to supersonic in the divergent portion, potentially generating shock waves in this portion and subsequently reverting to subsonic flow. All of these factors are primarily related to the chamber pressure-to-back pressure ratio [28].

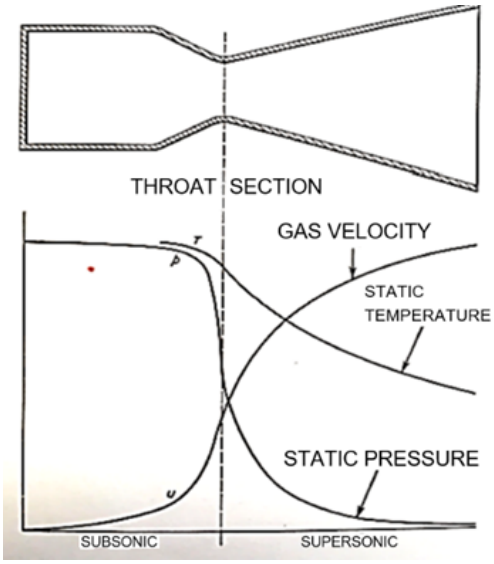

Figure 2. Static pressure, static temperature, and Mach number along nozzle

2.1 Nozzle Design Using Characteristic Curves Method

The Method of Characteristics (MOC) provides an effective framework for generating smooth, shock-free contours for supersonic nozzles. For an isentropic two-dimensional supersonic flow, the Prandtl–Meyer function $v(M)$ defines the turning angle required to expand the flow from Mach 1 at the throat to a desired exit Mach number Me. It is given by

$$v(\mathrm{M}) = \sqrt{\frac{\gamma+1}{\gamma-1}}\arctan\sqrt{\frac{\gamma+1}{\gamma-1}\left(\mathrm{M}^2-1\right)} - \arctan\sqrt{\left(\mathrm{M}^2-1\right)} \tag{1}$$

On each characteristic line, there is a constant value K that satisfies the compatibility condition, given for each line by the relationship [18]:

$$K+ = \theta - v(\mathrm{M}) \tag{2}$$

$$K- = \theta + v(\mathrm{M}) \tag{3}$$

where, θ is the flow turning angle. These relations are used to construct a characteristic mesh extending from the sonic line at the throat to the nozzle exit. By enforcing the condition that all expansion waves terminate at the centerline and no reflected waves reach the exit, a smooth-wall contour is generated that yields shock-free, fully isentropic expansion.

The MOC procedure used in this work follows standard nozzle-design formulations available in classical references such as Anderson [28] and Hoffman and Chiang [29]. The implemented MATLAB routine computes the wall coordinates by marching through the characteristic net, beginning with the initial expansion from the sonic throat and continuing until the desired exit Mach number is reached. The resulting contour ensures uniform exit flow and minimizes total-pressure losses.

Knowing the Mach number at the nozzle exit and the radius of the nozzle neck, the diverging part of the nozzle can be designed to be free of any form of shock at the nozzle exit.

The value of the Mach number at the exit can be calculated according to the following relationships [28]:

$$P_r = \frac{P_o}{P_c} \tag{4}$$

$$T_r = P_r^{\frac{\gamma-1}{\gamma}} \tag{5}$$

$$T_{cr} = \frac{2\gamma R T_c}{\gamma - 1} \tag{6}$$

$$P_{cr} = \left[\left(\frac{2}{\gamma - 1}\right)^{\frac{\gamma}{\gamma-1}}\right] 2.068 \tag{7}$$

$$V_{cr} = \sqrt{\frac{2\gamma R T_c}{\gamma + 1}} \tag{8}$$

$$V_e = \sqrt{T_{cr}\left(1 - \mathrm{T}_r\right)} \tag{9}$$

$$T_e = T_c \left(\frac{P_o}{P_c}\right)^{\frac{\gamma-1}{\gamma}} \tag{10}$$

$$C_e = \sqrt{\gamma R T_e} \tag{11}$$

$$M_e = \frac{V_e}{C_e} \tag{12}$$

where, P_r is pressure ratio, P_o is ambient pressure, P_c is chamber pressure, T_r is temperature ratio, γ is specific heat ratio and equal 1.4 for air, R is gas constant, T_{cr} is critical temperature at throat, T_c is chamber temperature, P_{cr} is critical pressure at throat, V_{cr} is velocity at throat, V_e is velocity at nozzle exist, T_e is temperature at nozzle exist, C_e is velocity of sound at nozzle exists, and M_e is Mach number at nozzle exists [30].

The conditions for the surrounding medium at altitude can be calculated from the relationships.

For $h >$ 25,000 m, corresponding to the upper stratosphere [18].

$$T(\mathrm{C}) = -131.21 + 0.0299h \tag{13}$$

$$P = 1000 \times 2.488 \left[\frac{T + 273.1}{216.6}\right]^{-11.388} \tag{14}$$

For 11,000 m $< h <$ 25,000 m agree to the lower stratosphere [17]:

$$T = -56.46C \tag{15}$$

$$P_o = 1000 \times 22.65 \times e^{(1.73 - 0.000157\ \mathrm{h})} \tag{16}$$

For $h <$ 11,000 m corresponding to troposphere [18].

$$T(\mathrm{C}) = 15.04 - 0.00649h \tag{17}$$

$$P = 1000 \times 11.29 \left[\frac{T + 273.1}{288.08}\right]^{5.256} \tag{18}$$

2.2 Mathematical Model

The numerical simulation was performed by solving the compressible Navier–Stokes equations together with the energy equation and turbulence transport equations. Because the flow inside the nozzle is supersonic and strongly compressible, a density-based solver was selected, which is appropriate for capturing shock waves, rapid density variations, and high-Mach-number effects [31].

2.3 Continuity Equation

It shows the law of conservation of mass:

$$\frac{\partial \rho}{\partial t} + \frac{\partial(\rho u)}{\partial x} + \frac{\partial(\rho v)}{\partial y} + \frac{\partial(\rho w)}{\partial z} = 0 \tag{19}$$

where, ρ represents density. u, v, w are components of the velocity on the x, y, and z directions respectively [32].

2.4 Momentum Equations

This indicates the mathematical significance of Newton's 2nd Law, momentum equation with respect to the x-axis [28]:

$$\left(\frac{\partial(\rho u)}{\partial t} + u\frac{\partial(\rho u)}{\partial x} + v\frac{\partial(\rho u)}{\partial y} + w\frac{\partial(\rho u)}{\partial z}\right) = -\frac{\partial p}{\partial x} + \rho g_x + \mu\left(\frac{\partial^2 u}{\partial x^2} + \frac{\partial^2 u}{\partial y^2} + \frac{\partial^2 u}{\partial z^2}\right) \tag{20}$$

Momentum equation on the y-axis:

$$\left(\frac{\partial(\rho v)}{\partial t} + u\frac{\partial(\rho v)}{\partial x} + v\frac{\partial(\rho v)}{\partial y} + w\frac{\partial(\rho v)}{\partial z}\right) = -\frac{\partial p}{\partial y} + \rho g_y + \mu\left(\frac{\partial^2 v}{\partial x^2} + \frac{\partial^2 v}{\partial y^2} + \frac{\partial^2 v}{\partial z^2}\right) \tag{21}$$

Momentum equation on the z-axis:

$$\left(\frac{\partial(\rho w)}{\partial t} + u\frac{\partial(\rho w)}{\partial x} + v\frac{\partial(\rho w)}{\partial y} + w\frac{\partial(\rho w)}{\partial z}\right) = -\frac{\partial p}{\partial z} + \rho g_z + \mu\left(\frac{\partial^2 w}{\partial x^2} + \frac{\partial^2 w}{\partial y^2} + \frac{\partial^2 w}{\partial z^2}\right) \tag{22}$$

where, P corresponds to pressure, g relates to the acceleration of gravity, and denotes viscosity as was provided according to the Sutherland correlation [21] in the viscous heating model.

3 Energy Conservation Equation

$$\underbrace{\frac{\partial(\rho e)}{\partial t}}_{1} + \underbrace{\vec{\nabla}\left(\rho\overrightarrow{\mathrm{V}}\ \mathrm{h}_o\right)}_{2} = \underbrace{\vec{\nabla}(\mathrm{K}\vec{\nabla}\ \mathrm{T})}_{3} + \underbrace{\vec{\nabla}(\tau\overrightarrow{\mathrm{V}})}_{4} + \underbrace{\overrightarrow{\mathrm{F}}_b\vec{V}}_{5} + \underbrace{\dot{Q}}_{6} \tag{23}$$

where, e is the internal energy [29]:

$$e = h - P/\rho + 1/2V^2 \tag{24}$$

where, h is the enthalpy, h_o is the stagnation enthalpy, τ is the shear stress [29].

The first term represented the mass's energy's time rate of change. The second term represented the energy carried away by the flow to and from the fluid's main body due to movement of fluid. The third term represented the energy conducted into the system. The fourth term represented energy lost in the bulk because of viscosity. The fifth term represented the power that was thematically circulated in and out of the system through the volumetric forces that were exerted upon it. The sixth term represented the heating of the system because of the presence of an internal heat source [21].

Turbulence was modeled using the $k-\omega$ SST (M stress transport) model, which combines the near-wall accuracy of the standard $k-\omega$ formulation with the free-stream robustness of the $k-\omega$ model. This model is widely recommended for internal compressible flows with strong adverse pressure gradients and potential shock–boundary-layer interaction—conditions typical of ramjet and discharging coefficient (DC) nozzles. The SST formulation improves prediction of separation and wall heat transfer and is therefore suitable for the present thermal–aerodynamic analysis.

Air was treated as an ideal compressible gas with temperature-dependent viscosity using Sutherland's law. Second-order discretization schemes were applied to all governing equations to ensure adequate resolution of shocks and steep gradients.

3.1 Geometry

The diverging portion of the nozzle is designed according to the pressure and temperature conditions of the chamber shown in the Table 1.

The nozzle was drawn and designed using the characteristic curves method. The code was written in MATLAB and the coordinates of the points on the nozzle wall were determined as shown in the diagram and Figure 3 and Figure 4. Then the nozzle was drawn using Solidworks.

The studied geometric model represents the fluid field within the nozzle and the surrounding fluid, where the studied fluid is air as an ideal compressible gas whose properties are shown in the Table 2.

Figure 5 shows the studied geometric model with the dimensions obtained for the diverging part using the characteristic curves method.

Table 1. The pressure and temperature conditions of the chamber

Parameter	Value
Chamber pressure	2.27 MPa
Chamber temperature	1200 K
Altitude	7500 m
Specific heat ratio	1.4
Gas constant	355 J/(kg·K)

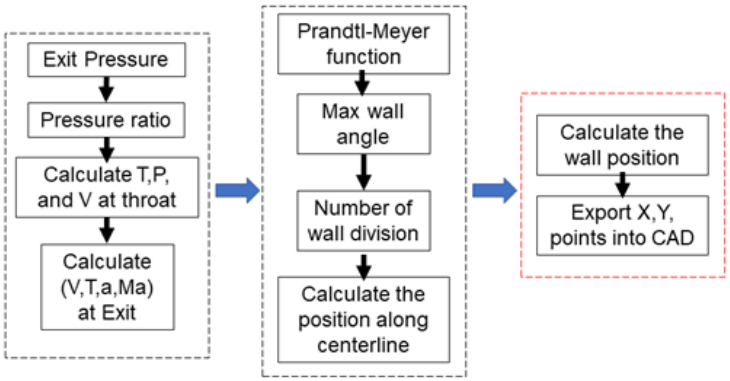

Figure 3. Matrix Laboratory (MATLAB) flow chart to determine the coordinates of the points on the nozzle wall

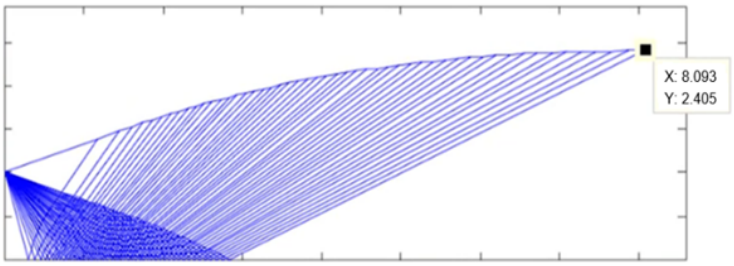

Figure 4. Characteristic curve getting for 50 division

Table 2. Physical properties of air

Unit	Value	Quantity
kg/m^3	Ideal gas law	Density ρ
J/(kg·K)	1006.43	Heat capacity c_p
Pa·s	Sutherland	Viscosity μ

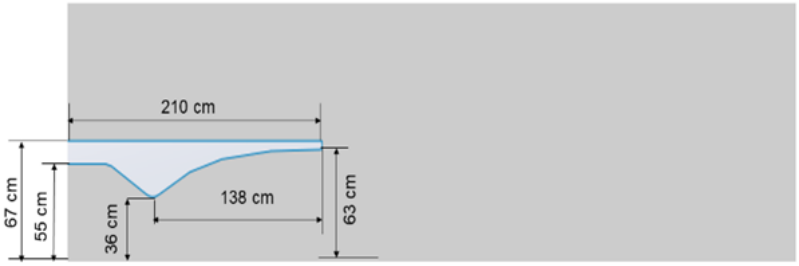

Figure 5. Dimension of studied fluid domain

3.2 Boundary Condition

In supersonic nozzle simulations where the flow is choked at the throat, the outlet static pressure becomes the primary parameter controlling whether the flow is over-expanded, ideally expanded, or under-expanded. Therefore,

in addition to specifying the total pressure and total temperature at the inlet, the static pressure at the outlet must be explicitly imposed. In this study, the outlet static pressure was defined based on the ambient atmospheric pressure corresponding to the operating altitude (7,500 m). This static pressure was then varied according to the chamber-to-ambient pressure ratio examined in the parametric study. These variations in backpressure are the main driver of the flow structure inside the nozzle, shock formation, and thrust coefficient (TC) behavior.

To solve any differential equation, appropriate boundary conditions are required to solve the mathematical model. The Figure 6 represents the location and type of these conditions, while the Table 3 represents their values.

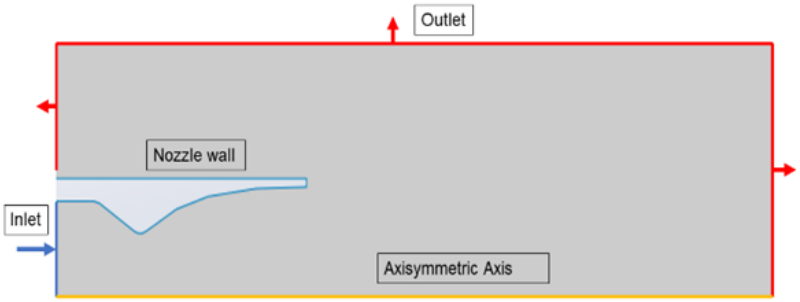

Figure 6. Boundary condition

Table 3. Values of boundaries condition

Value	Boundary Condition	Surface
Chamber pressure	Total pressure inlet	Inlet
Chamber temperature	Total temperature inlet	Inlet
Static pressure according to altitude	Pressure outlet	Outlet
$\vec{V} = 0$	No slip condition	Wall

3.3 Mesh and Mesh Independence Study

Accurate resolution of shocks and steep gradients in supersonic nozzle flows requires a sufficiently refined mesh, particularly near the throat and in regions where shock interactions may occur. Although adaptive mesh refinement (AMR) was employed during the solution process to capture local gradients, a conventional mesh independence assessment was still performed to ensure that both the initial mesh and refinement settings were adequate.

An initial structured/unstructured hybrid mesh was generated with targeted refinement in the throat and early divergent region. Three baseline mesh levels (coarse, medium, and fine) were tested prior to enabling AMR. The medium and fine meshes showed less than 2% variation in mass flow rate and TC, indicating satisfactory mesh convergence. Based on this result, the medium mesh was selected as the starting grid.

During the simulation, AMR was applied based on pressure-gradient criteria to resolve shock locations as they shifted with the chamber-to-ambient pressure ratio. To confirm that AMR did not introduce dependency on refinement cycles, the final mesh distribution of each case was compared to the pre-refined fine grid, showing consistent shock structure and less than 1% deviation in the computed TC. Figure 7 shows the initial mesh used in the solution.

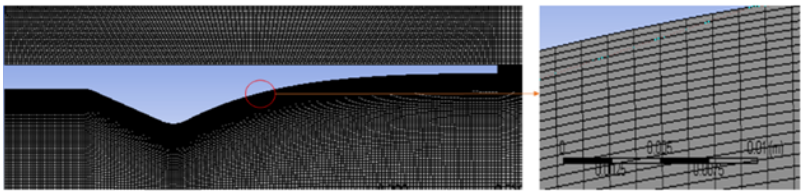

Figure 7. Initial mesh used in the solution

Thus, both the initial mesh sensitivity test and the consistency of AMR-refined meshes confirm that the adopted meshing strategy provides sufficient accuracy for the present study.

3.4 Solution Strategy and Validation

In order to solve the required mass conservation, momentum and energy equations, the density -based solver was chosen as a method to velocity-pressure coupling with second order discretization for all equations, the mass

conservation equation residuals were adjusted until 10^{-6} while energy equations were set to 10^{-8}.

To verify the accuracy of the numerical approach and the physical models used, the present simulation was validated against the experimental nozzle data reported by Thornock and Brown [32]. The reference nozzle has a comparable geometry and operating conditions, including a choked throat and a supersonic divergent region, making it suitable for assessing the solver's ability to capture shock location, Mach distribution, and pressure variation along the centerline.

The validation procedure consisted of reproducing the experimental inlet total pressure and temperature, applying the same ambient backpressure, and meshing the nozzle with the same refinement strategy used in the main study. The resulting pressure distribution along the nozzle axis was extracted and compared with the experimental measurements.

Figure 8 shows that the numerical results closely follow the experimental trends, particularly in predicting (i) the pressure drop upstream of the throat, (ii) the rate of expansion in the divergent portion, and (iii) the location and strength of internal shock structures. The maximum deviation between numerical and experimental pressure values remained within 5%, which is consistent with typical uncertainties for compressible-flow computational fluid dynamics simulations of supersonic nozzles. The accurate capture of shock position confirms the suitability of the density-based solver and the $k-\omega$ SST turbulence model for resolving the flow physics relevant to the present work.

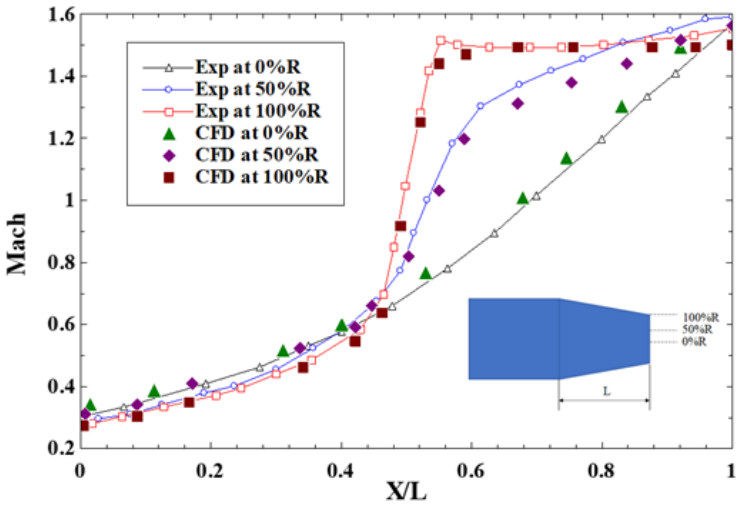

Figure 8. Model validation

4 Results and Discussion

Ensuring the proper design of a nozzle for specific flow conditions requires ensuring that the flow area within the nozzle is free of any shocks. This requires studying the performance and operation of this nozzle at different pressure ratios by studying the change in the value of the thrust and discharge coefficient with the change in the pressure ratio. The DC is defined as the actual mass flow divided by the ideal mass flow and TC is defined as the actual thrust divided by the ideal thrust. Figure 9 displays the change in the value of these two parameters as the pressure ratio changes.

We note that the change in the value of the Discharge coefficient reaches a constant value at a compression ratio of 44.23, where the flow exiting the nozzle at a compression ratio value lower than this value is supersonic, but it is over-expansion. After this value, the flow becomes under-expansion. Therefore, we note that the value of this coefficient at a compression ratio of 44.23 has become constant and does not change, and the ratio of this coefficient is 0.92. Although the flow at the neck reaches sonic flow conditions and turns into supersonic in the diverging part of the nozzle, the flow conditions cannot reach isentropic flow conditions in the entire diverging part except under specific conditions. This can be observed from the curve of change of TC with compression ratio, where we notice from this curve the presence of a single optimal value at a compression ratio of 57, where the value of TC is maximum and reaches 0.968. This value matches the conditions of shock-free isentropic flow in the entire diverging part. We notice a decrease in the value of this coefficient with the increase in the value of the compression degree due to the formation of shocks that lead to large losses in the flow and thus a decrease in the value of the thrust produced by the nozzle.

After reaching the design pressure ratio, the flow at the outlet becomes higher than atmospheric pressure, resulting in an under-expanded flow. This leads to the formation of expansion waves and strong shocks outside the nozzle, causing a drop in total pressure and losses in axial momentum. Although the mass flow rate remains constant

(because the throat is constricted), the shock losses reduce the effective impulse, and the impulse coefficient Ct falls below its optimum value.

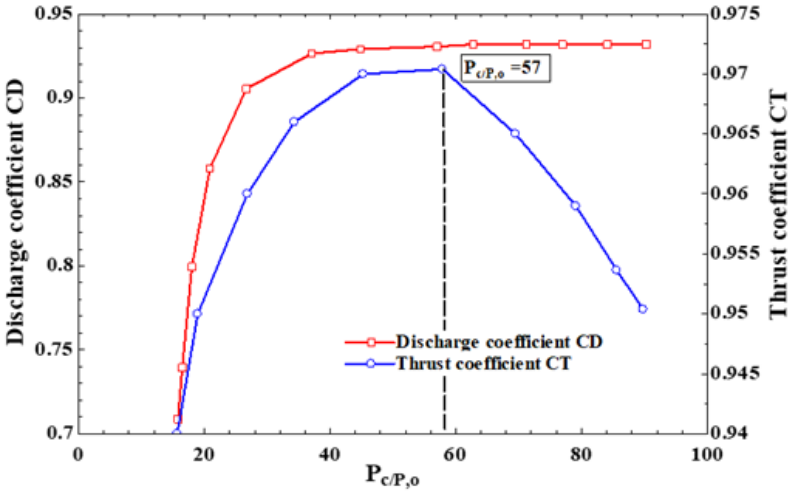

Figure 9. Discharge and thrust coefficient (TC)

The Figure 10, Figure 11, Figure 12, Figure 13, and Figure 14 show the variations in Mach number, static pressure, and temperature across the nozzle at a compression ratio of 57. The previous Figures also show the pressure, temperature, and Mach number plots at the same pressure.

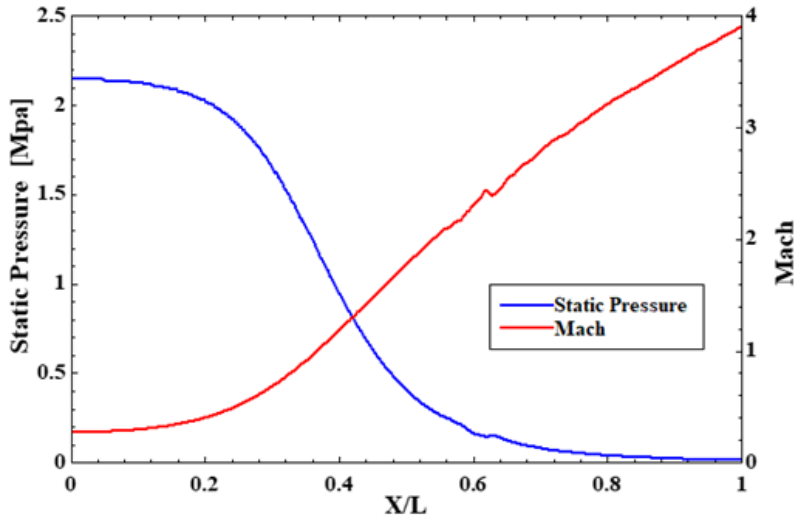

Figure 10. Static pressure and Mach number variation along nozzle

We observe that the static pressure and temperature continue to decrease across the nozzle's length, while the Mach number increases. The flow is subsonic in the convergent portion of the nozzle. At the neck, the Mach number reaches 1, and the flow in the divergent portion turns supersonic as the Mach number increases. The Mach number reaches 1 near the neck of the nozzle, where the flow is throttled. The flow in the divergent portion of the nozzle remains supersonic, achieving the conditions for isentropic flow, free of vertical shocks that cause flow interruptions and losses, which drain the flow's energy.

The flow regions within the divergent part of the nozzle and outside the nozzle can be analyzed from the Figure 15 that shows the value of the Mach number within the studied range.

The image shows the structure of a supersonic jet resulting from the exit of high-pressure gas from a nozzle into a low-pressure surrounding medium, a condition known as an under-expanded jet. At the nozzle exit, the pressure inside the nozzle is higher than the external atmospheric pressure, leading to the formation of expansion waves as the gas is forced out of the nozzle. These waves radiate outward from the nozzle edge to relieve pressure and accelerate the flow. the result of the gases expanding , the jet starts to show a repeating pattern of expansion and compression zones along its axis.

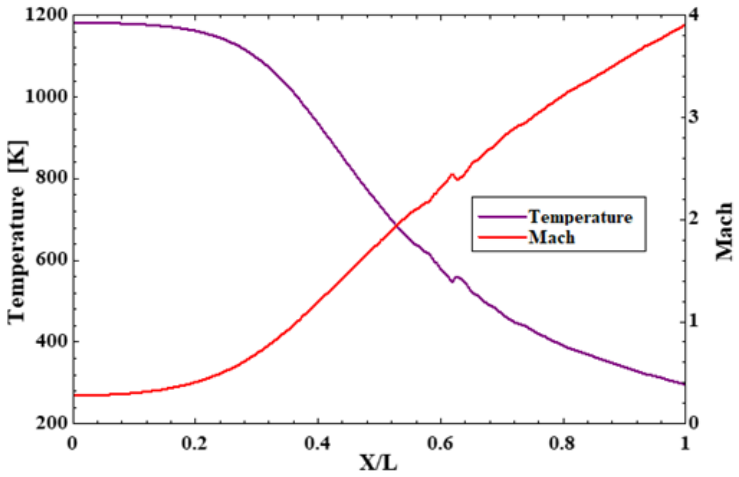

Figure 11. Static temperature and Mach number variation along nozzle

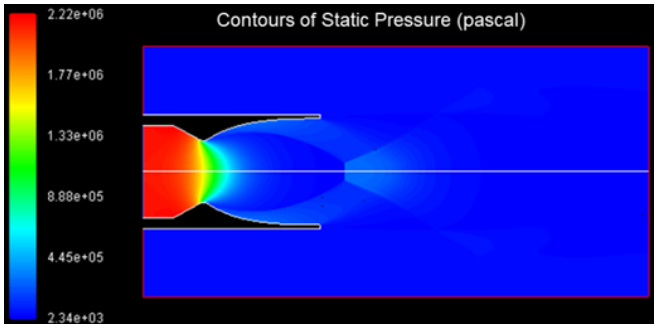

Figure 12. Contours of static pressure

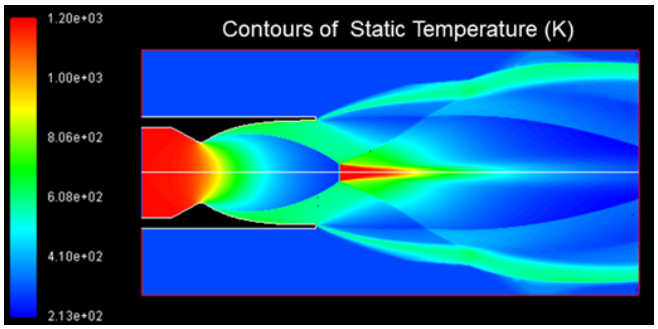

Figure 13. Contours of static temperature

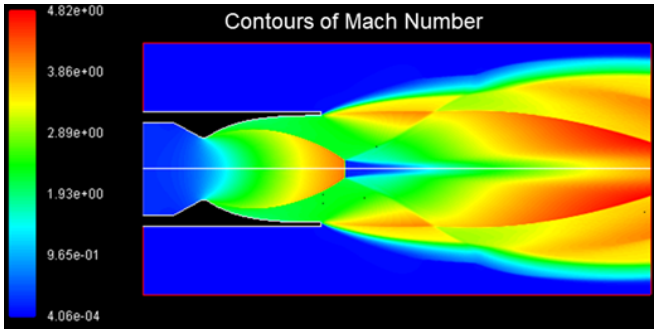

Figure 14. Contours of Mach number

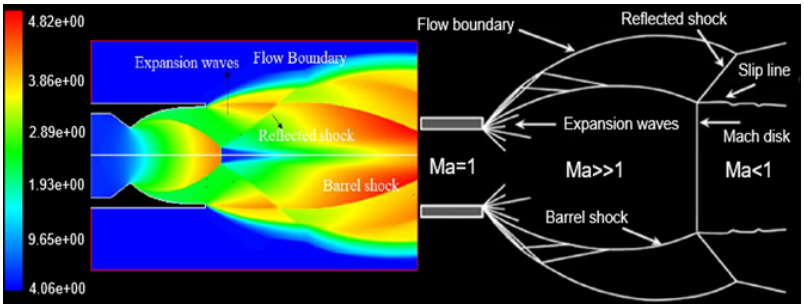

Figure 15. Flow regions within the divergent part of the nozzle and outside the nozzle

After the expansion waves pass, the flow becomes compressed more than needed, and this creates a set of oblique shocks around the jet. they form a barrel shock. At the centerline, these shocks meet and create a vertical shock known as a Mach disk.

Here, the flow shifts suddenly from supersonic to subsonic and both pressure and temperature rise in a noticeable way.

After that, the shocks reflect outward and flow tries to settle back toward a state that may be closer to acceptable equilibrium. A slip line forms between regions of the flow that have different speeds and thermal conditions.

This repeating pattern, made of shocks and expansion zones, is known as a shock-cell structure. It is one of the clearer signs of a non-expansive supersonic jet.

The nozzle was designed with MOC to generate isentropic expansion up to an output Mach number ≈ 3.29, i.e., at a design compression ratio ≈ 56.7 (approximately 57). The key finding in the results—that the optimal value of the pressure ratio is 57—is directly related to this design ratio. This clearly justifies that the optimal state observed in the simulation does indeed represent the design state upon which the nozzle was built.

5 Conclusion

Key outcomes of this study can be summarized as follows:

• A supersonic ramjet nozzle was successfully designed using the MOC to achieve smooth, shock-free expansion at the target operating pressure ratio.

• Numerical results showed that the optimal chamber-to-ambient pressure ratio is $\approx$57, which matches the design condition and yields the maximum TC.

• For pressure ratios lower than this value, the nozzle operates in an over-expanded regime, while higher ratios lead to under-expanded flow and shock-induced total-pressure losses.

• Contours of pressure, temperature, and Mach number confirmed the expected flow behavior and validated the fidelity of the numerical model.

Overall, the designed contour demonstrated its ability to sustain uniform supersonic flow and maximize thrust under the intended operating condition.

Limitations and potential future work include:

• Extending the analysis to 3D geometries to capture side-wall effects and asymmetry in the jet plume.

• Investigating material–thermal response and fluid-structure interaction under long-duration operation.

• Studying off-design performance using variable backpressure profiles representing realistic flight trajectories.

• Exploring alternative nozzle contours (e.g., dual-bell, aerospike) for improved adaptability to altitude variations.

We observe a high agreement between the experimental and numerical results, which indicates that the physical model used and the solution strategy followed give correct results.

This agreement demonstrates that the computational setup, meshing strategy, and physical models yield reliable predictions for the operating regime analyzed in this study.

Data Availability

The data used to support the findings of this study are available from the corresponding author upon request.

Conflicts of Interest

The authors declare that they have no conflicts of interest.

References

[1] W. Heiser, D. Pratt, D. Daley, and U. Mehta, *Hypersonic Airbreathing Propulsion*. American Institute of Aeronautics and Astronautics, Inc., 1994.

[2] S. M. Neill and A. Pesyridis, "Modeling of supersonic combustion systems for sustained hypersonic flight," *Energies*, vol. 10, no. 11, p. 1900, 2017. https://doi.org/10.3390/en10111900

[3] S. Ekanayake, J. A. Gear, and Y. Ding, "Flow simulation of a two dimensional rectangular supersonic convergent divergent nozzle," *ANZIAM J.*, vol. 51, pp. 377–392, 2009. https://doi.org/10.21914/anziamj.v51i0.2577

[4] O. J. Haidn, "Advanced rocket engines," in *Advances on Propulsion Technology for High-Speed Aircraft*. North Atlantic Treaty Organization, 2007, pp. 6.1–6.40.

[5] R. Svoboda, "Mission analysis and feasibility study for the recovery system of a suborbital rocket," mastersthesis, École Polytechnique Fédérale de Lausanne (EPFL), Lausanne, Switzerland, 2025. https://espace.epfl.ch/wp-content/uploads/2025/07/Mission-Analysis-and-Feasibility-Study-for-the-Recovery-System-of-a-Suborbital-Rocket.pdf

[6] P. D. Malali, "Prediction of shock diamonds and mach disk in an under-expanded air jet," mastersthesis, Old Dominion University, 2010. https://doi.org/10.25777/vd0w-zf35

[7] G. Hagemann, H. Immich, T. Van Nguyen, and G. E. Dumnov, "Advanced rocket nozzles," *J. Propuls. Power*, vol. 14, no. 5, pp. 620–634, 1998. https://doi.org/10.2514/2.5354

[8] J. Thongsri, K. Srathonghuam, and A. Boonpan, "Gas flow and ablation of 122 mm supersonic rocket nozzle investigated by conjugate heat transfer analysis," *Processes*, vol. 10, no. 9, p. 1823, 2022. https://doi.org/10.3390/pr10091823

[9] B. G. Sheikh, R. Kumar, and S. K. S, "Coupled flow-thermal analysis of a rocket nozzle with charring ablative thermal protection system," *arXiv preprint arXiv:2411.19792*, 2025. https://doi.org/10.48550/arXiv.2411.19792

[10] R. Li, J. Xu, H. Lv, D. Lv, and J. Song, "Numerical investigations of the nozzle performance for a rocket-based rotating detonation engine with film cooling," *Aerosp. Sci. Technol.*, vol. 136, p. 108221, 2023. https://doi.org/10.1016/j.ast.2023.108221

[11] J. Braun and G. Paniagua, "Rotating detonation combustor operability and aero-thermal performance with an integrated diverging nozzle," *Appl. Therm. Eng.*, vol. 249, p. 123126, 2024. https://doi.org/10.1016/j.applthermaleng.2024.123126

[12] V. S. Zakharov, O. V. Guskov, A. N. Prokhorov, and V. N. Berezhnoy, "Computational and experimental study of the influence of the shape of nozzle supersonic part on the flow structure in the gas-dynamic flow path of a model high-altitude test facility," *Thermophys. Aeromech.*, vol. 28, no. 2, pp. 153–173, 2021. https://doi.org/10.1134/S0869864321020013

[13] Y. Guan, S. Becker, and D. Zhao, "Research and development on ramjet combustion instabilities," *J. Therm. Sci.*, vol. 34, pp. 689–706, 2025. https://doi.org/10.1007/s11630-025-2103-8

[14] A. Govindraju, S. Kumar, T. Pachauri, K. Awasthi, N. U. Shetty, V. Singh, and K. Manoj, "Flow analysis of ramjet engine for optimized nose cone design," in *Proceedings of the 2nd Indian International Conference on Industrial Engineering and Operations Management*, Warangal, India, 2022, pp. 926–937. https://doi.org/10.46254/IN02.20220268

[15] A. Albadwi, A. Faisal, M. Abdelhalim, A. Salih, M. Khalil, and O. Musa, "Design and analysis of an air intake system of ramjet engine using CFD simulations," *Int. J. Eng. Inf. Syst.*, vol. 5, no. 2, pp. 180–190, 2021, no DOI or official URL available.

[16] R. Baidya, A. Pesyridis, and M. Cooper, "Ramjet nozzle analysis for transport aircraft configuration for sustained hypersonic flight," *Appl. Sci.*, vol. 8, no. 4, p. 574, 2018. https://doi.org/10.3390/app8040574

[17] K. S. Naidu and D. K. Bajaj, "Modelling and exhaust nozzle flow simulations in a scramjet," *J. Astrophys. Aerosp. Technol.*, vol. 3, no. 2, p. 1000122, 2015.

[18] T. Le Pichon and A. Laverdant, "Numerical simulation of reactive flows in ramjet type combustors and associated validation experiments," *J. Aerosp. Lab*, vol. 11, p. 3, 2016. https://doi.org/10.12762/2016.AL11-03

[19] A. Kozelkov, A. Struchkov, A. Kornev, and A. Kurkin, "A numerical approach and study of the shock-wave structure of supersonic jet flow in a nozzle," *Fluids*, vol. 9, no. 7, p. 164, 2024. https://doi.org/10.3390/fluids9070164

[20] G. Wang, J. Zou, L. Chen, and B. Guan, "Parametric study on configuration geometry effect on thrust performance of annular ED nozzles," *Propuls. Energy*, vol. 1, no. q, p. 2, 2025. https://doi.org/10.1007/s44270-024-00007-1

[21] T. H. Shieh, K. W. Lin, and Y. T. Li, "Flow effects and propulsion performance on various single expansion ramp nozzle configurations of scramjet engine," *Symmetry*, vol. 16, no. 8, p. 1044, 2024. https://doi.org/10.3390/sym16081044

[22] D. Wang, D. Cao, Z. Zhou, and R. Liang, "Numerical simulation of fluid–structure interaction for solid rocket engine nozzle ablation," *Adv. Aerodyn.*, vol. 7, no. 1, p. 2, 2025. https://doi.org/10.1186/s42774-024-00192-2

[23] K. Schomberg, J. Olsen, and G. Doig, "Analysis of a low-angle annular expander nozzle," *Shock Vib.*, vol. 2015, no. 1, p. 675861, 2015. https://doi.org/10.1155/2015/675861

[24] K. M. Pandey and B. Nath, "Numerical simulation of a hydrogen fueled scramjet combustor at Mach 1.5 using strut injectors at Mach 2.47 air speed," in *Proceedings of the ASME 2013 International Mechanical Engineering Congress and Exposition*, San Diego, California, USA, 2013. https://doi.org/10.1115/IMECE2013-66036

[25] G. Hagemann and M. Frey, "Shock pattern in the plume of rocket nozzles: Needs for design consideration," *Shock Waves*, vol. 17, no. 6, pp. 387–395, 2008. https://doi.org/10.1007/s00193-008-0129-y

[26] J. W. Connolly, D. J. Friedlander, and G. Kopasakis, "Computational fluid dynamics modeling of a supersonic nozzle and integration into a variable cycle engine model," in *Proceedings of the 50th AIAA/ASME/SAE/ASEE Joint Propulsion Conference*, Cleveland, OH, USA, 2014, p. 3687. https://doi.org/10.2514/6.2014-3687

[27] D. Munday, E. Gutmark, J. Liu, and K. Kailasanath, "Flow structure and acoustics of supersonic jets from conical convergent-divergent nozzles," *Phys. Fluids*, vol. 23, no. 11, p. 116102, 2011. https://doi.org/10.1063/1.3657824

[28] J. D. Anderson, *Computational Fluid Dynamics: The Basics with Applications*. New York: McGraw-Hill, 2002.

[29] K. A. Hoffmann and S. T. Chiang, *Computational Fluid Dynamics Volume 1*. Engineering Education System, 2000.

[30] ANSYS, *ANSYS Fluent theory guide*, 2025. https://ansyshelp.ansys.com/public//Views/Secured/corp/v252/en/pdf/Ansys_Fluent_Theory_Guide.pdf

[31] ANSYS, *ANSYS Fluent user's guide*, 2025. https://ansyshelp.ansys.com/public//Views/Secured/corp/v252/en/pdf/Ansys_Fluent_Users_Guide.pdf

[32] R. L. Thornock and E. F. Brown, "An experimental study of compressible flow through convergent-conical nozzles, including a comparison with theoretical results," *J. Fluids Eng.*, vol. 94, no. 4, pp. 926–930, 1972. https://doi.org/10.1115/1.3425591